

Elevation Analysis for Urban Microcell Outdoor Measurements at 2.3 GHz

Antti Roivainen*, Veikko Hovinen*, Juha Meinilä[†]*, Nuutti Tervo*, Marko Sonkki*, Claudio Ferreira Dias*

*Department of Communications Engineering (DCE) & Centre for Wireless Communications (CWC),
P.O. Box 4500, 90014 University of Oulu, Finland

[†]Elektrobit Wireless Communications Ltd, Tutkijantie 7, 90570 Oulu, Finland

Email:{antti.roivainen, veikko.hovinen, nutervo, msonkki, cferreir}@ee.oulu.fi and Juha.Meinila@elektrobit.com

Abstract—This paper presents the analysis of departure elevation angles for the urban microcell radio channel measurements at 2.3 GHz. The measurements were conducted with EB Propsound CSTM for 30 x 16 antenna configuration in Oulu city center, Finland. The transmitter (Tx) antenna heights of 5 m and 10 m were used. The Tx antenna elements were arranged in the plus shape and nine antenna elements were placed with linear spacing in the vertical dimension providing high elevation resolution and an accurate elevation angle estimate for the departure angles. The measurement results indicate that the Laplacian distribution can be used for modelling the elevation angles of departure. A smaller elevation spread of departure (ESD) is observed for the higher Tx antenna height. Furthermore, a significant difference in ESDs between the line-of-sight (LOS) and the non-line-of-sight (NLOS) propagation environments are noticed. The ESD with respect to distance is observed to follow the negative exponential model and the linear model in the LOS and the NLOS propagation environments, respectively.

I. INTRODUCTION

Two dimensional (2D) channel models, e.g., WINNER II [1] and International Telecommunication Union radiocommunication sector (ITU-R) channel model [2], have been accurate enough in the fourth generation (4G) wireless communication studies. The effect of radio wave propagation in the elevation domain was assumed to be negligible in these models. However, the wireless communication traffic is expected to grow explosively in the next few years and more advanced channel models are needed for the fifth generation (5G) mobile and wireless communication systems. To meet this demand, the higher frequencies and wider bandwidths should be utilized. Furthermore, the resources of the current spectrum should be exploited maximally. Therefore, an accurate three-dimensional (3D) multiple-input multiple-output (MIMO) geometry based stochastic channel model (GSCM) is needed for the elevation domain beamforming and spatial multiplexing.

The analysis of radio wave propagation in the elevation domain has gained a lot of interest in the past few years. Several measurement campaigns have been carried out and the angular characteristics in the elevation domain have been investigated, e.g., in [3], [4]. The 3D extension of ITU-R channel model was proposed in [5]. However, according to the best knowledge of the author's, the majority of the existing work in the analysis of elevation domain has been focused on the macrocell environment and only a few works, e.g., [6], [7], have been concentrating on the analysis of elevation dimension

in microcell. In [8], the elevation angle parameters are reported for urban microcell (UMi) but the elevation resolution is limited by the measurement data, i.e., the analysis in the elevation domain, especially at the base station (BS), is based on measurements where the number of antenna elements in the vertical domain is small.

This motivated us to perform radio channel measurements in a microcell environment. This paper concentrates on the analysis of the elevation angles of departure (EoD) and the elevation spread of departure (ESD). In order to achieve an accurate elevation resolution at the transmitter (Tx), i.e., at the BS, nine antenna elements were placed with linear spacing in the vertical dimension. Therefore, this paper provides more accurate elevation angle estimates for the propagated paths against the majority of the existing measurement results.

The rest of the paper is organized as follows. In Section II, the measurement equipment and environment are described. Section III presents the theory of elevation angle analysis and the measurement results. Finally, the conclusions are drawn in Section IV.

II. MEASUREMENT EQUIPMENT AND ENVIRONMENT

The measurements were conducted with EB Propsound CSTM [9] at the center frequency of 2.3 GHz. A uniformly spaced linear antenna array (ULA) was used as the Tx antenna and it was installed in an articulated crane in order to vary the Tx antenna height. The ULA consists of 15 dual polarized elements (30 feeds) and the elements of antenna array are arranged in the plus shape (Fig.1a). The Tx antenna heights were 5 meters and 10 meters above the street level in the measurements. An omnidirectional antenna array (ODA) was used as the receiver (Rx) antenna (Fig.1b) and it was installed on the roof of a car at the height of 2.5 m above the street level. The measurement device uses direct sequence spread spectrum (DSSS) technique for channel sounding. The impulse responses (IRs) of channel samples are obtained by correlating the received signal with the spreading code used in transmission. Sounding in the spatial domain is achieved by switching through the multiple antennas in the time domain. The antenna elements are switched through in a such way that the channel response remains constant within antenna switching period.

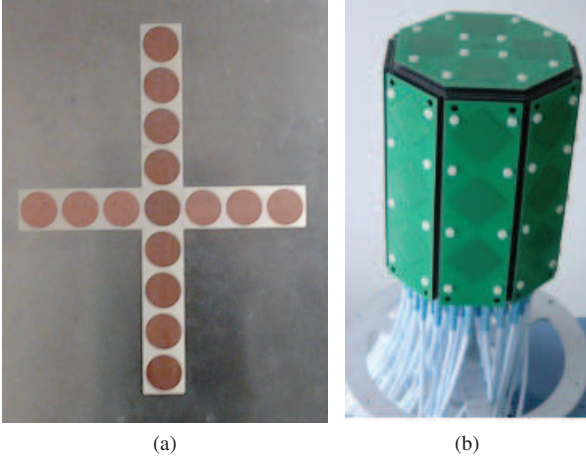


Fig. 1. (a) Tx antenna array (b) Rx antenna array.

TABLE I
MEASUREMENT SETTINGS

Center frequency [GHz]	2.3
Bandwidth [MHz]	100
Transmission power [dBm]	23
Antenna configuration	30 x 16
Code length [chips]	127
Measurable delay [μ s]	2.55
Array scan time [ms]	2.59
Channel coherence time [ms]	2.8
Snapshot duration [ms]	5.2

The antenna switching period should be shorter than channel coherence time. This sets the limitation to the useable antenna configuration for urban measurements where several moving scatterers are present. Therefore, the lowest ring of dual polarized patches in the azimuth domain, i.e., 16 ports were selected from the Rx antenna array for the measurements. This also indicates that the elevation spread of arrival (ESA) cannot be analyzed. The measurement settings are presented in the Table I.

The GPS positions of the Rx were recorded in order to calculate the distance between the Tx and the Rx. In addition, GPS data was recorded by a navigator and an external GPS device for cross-checking the Rx positions in the data analysis phase. The measurements were performed at Oulu city center. The Rx was immobile during the data recordings. Several spots including line-of-sight (LOS) and non-line-of-sight (NLOS) propagation conditions were recorded. The measurement routes are presented in Fig. 2.

III. DATA ANALYSIS AND MEASUREMENT RESULTS

The data analysis is divided into four group based on Tx antenna height and propagation environment, i.e., the data analysis is done independently for both Tx antenna heights and LOS and NLOS scenarios. The angular estimates and the powers of each individual paths were obtained by initialization and search improved SAGE (ISIS) algorithm [10].

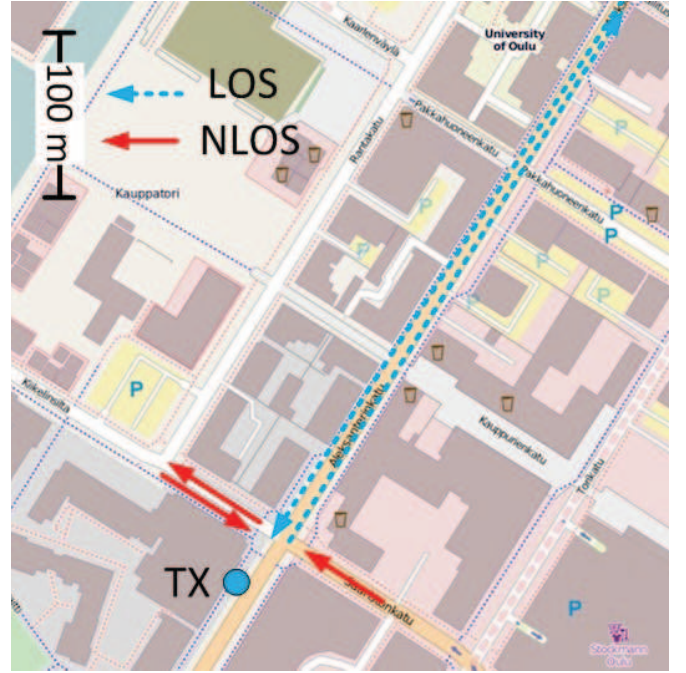


Fig. 2. Measurement routes.

A. EoD Distributions

The Laplacian distribution used for fitting the observed EoDs is presented as

$$f_{EoD}(\theta) = \frac{1}{\sqrt{2}\sigma_{EoD}} \exp\left(-\frac{|\sqrt{2}(\theta_m - \mu_{EoD})|}{\sigma_{EoD}}\right), \quad (1)$$

where θ_m is the EoD of the m th path and μ_{EoD} , σ_{EoD} are the mean and standard deviation of the Laplacian distribution, respectively. The mean of EoD is normalized to zero degree and the probability density function (PDF) for EoD is presented in Fig. 3. The Laplacian distribution fits fine for the observed EoDs in the NLOS scenario. In the LOS scenario, a small offset between the measured EoDs and the Laplacian distribution can be observed.

B. ESD Analysis

The ESD for each measured time instant is calculated as described in 3rd Generation Partnership Project spatial channel model (3GPP SCM) specification [11] from the EoDs and the path power values as

$$ESD = \min_{\Delta} \sigma_{AS}(\Delta) = \sqrt{\frac{\sum_{m=1}^M (\theta_m(\Delta) - \mu_{\theta}(\Delta))^2 \cdot P_m}{\sum_{m=1}^M P_m}}, \quad (2)$$

where Δ is a discrete grid for minimization, $\theta_m(\Delta) = \theta_m + \Delta$, P_m is the power of the m th path and $\mu_{\theta}(\Delta)$ is the mean of elevation angular power of departure calculated as

$$\mu_{\theta}(\Delta) = \frac{\sum_{m=1}^M \theta_m(\Delta) \cdot P_m}{\sum_{m=1}^M P_m}. \quad (3)$$

The cumulative density function (CDF) for the ESD is presented in Fig. 4. The difference between the LOS and

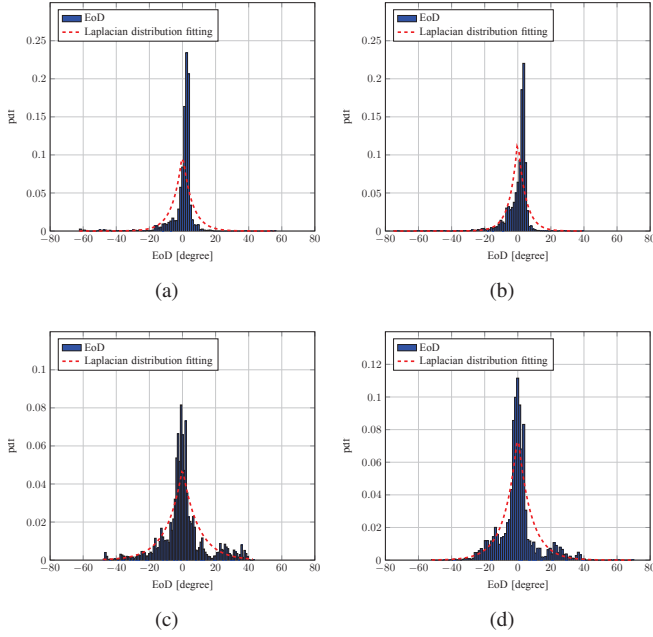


Fig. 3. PDF of EoD (a) LOS, Tx height 5 m (b) LOS, Tx height 10 m (c) NLOS, Tx height 5 m (d) NLOS, Tx height 10 m.

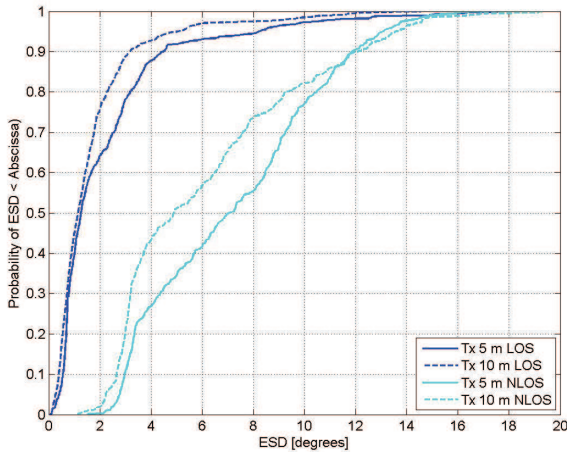


Fig. 4. CDF of ESD.

the NLOS scenario is clearly seen from the Fig. 4. The contribution of direct path in the LOS propagation condition is significantly higher than the contribution of multipath components (MPCs), which leads to smaller ESD in the LOS scenario. In the NLOS scenario, the ESD differs remarkably between the two Tx antenna heights. The reason for this is the fact that the stronger MPCs are detected from the ground reflection with the lower Tx antenna height.

C. ESD Distance Dependency Models

In this subsection, the ESD dependency on distance is investigated. The ESD with respect to the distance between the Tx and the Rx is tested against linear model and negative

exponential model. The linear model is presented as

$$ESD_{l,m}(d) = A_{l,m} + B_{l,m}d, \quad (4)$$

where $A_{l,m}$ and $B_{l,m}$ are the coefficients for the linear model obtained by using the least square (LS) method, d is the distance between the Tx and the Rx and the subscripts $\{l, m\}$ stands for linear and model, respectively. The negative exponential model is presented as

$$ESD_{n,e,m}(d) = A_{n,e,m} \cdot \exp(-B_{n,e,m}d), \quad (5)$$

where $A_{n,e,m}$ and $B_{n,e,m}$ are the coefficients for the negative exponential model and the subscripts $\{n, e, m\}$ stands for negative, exponential and model, respectively. In addition, the 3GPP model for the distance dependency of ESD [12] is plotted as the reference in Figs. 5–8. The models are compared to the measured ESDs by calculating the standard deviation, γ , between the model and the measured ESDs. Finally, the model which gives the smallest standard deviation is selected for the distance dependency model of ESD.

The ESD with respect to the distance between the Tx and the Rx for the LOS scenarios are presented in Figs. 5–6. In order to extract out the angular estimates using ISIS algorithm, approximately 15 dB dynamic range is needed, i.e., the difference between the highest peak and noise level in the IR should be at least 15 dB. On the radio link there is a small mound with the height of three meters approximately 150 meters away from the Tx. Due to diffraction loss, it causes a remarkable attenuation to the received power when the Tx antenna height is 5 meters. Therefore, the results for the Tx antenna height of 5 meters are presented only for distance range from 50 meters to 170 meters.

The standard deviation of 1.0 degrees and 0.6 degrees is observed for the linear model and the negative exponential model in the LOS scenario for the lower Tx antenna height, respectively. For the LOS scenario where the Tx antenna height is 10 meters, the standard deviation of 1.2 degrees and 0.9 degrees is achieved for the linear model and the negative exponential model, respectively. Therefore, the negative exponential model is selected for the ESD distance dependency model in the LOS scenario and the coefficients for the model are presented in Table II.

The ESD with respect to the link distance for NLOS scenarios are presented in Figs. 7–8. The standard deviation of 0.9 degrees and 1.0 degrees is obtained for the linear model and the negative exponential model in the NLOS scenario for the lower Tx antenna height, respectively. For the NLOS scenario where the Tx antenna height is 10 meters, the standard deviation is 1.2 degrees for both models. Because the linear model offers smaller standard deviation for the lower Tx antenna height in the NLOS scenario, it is selected also for NLOS scenario where the Tx antenna height is 10 meters. The coefficients for the linear model in the NLOS scenario are presented in Table II. The standard deviation between the selected model and the measured ESDs is larger for NLOS scenarios in comparison to LOS scenarios. This is partly

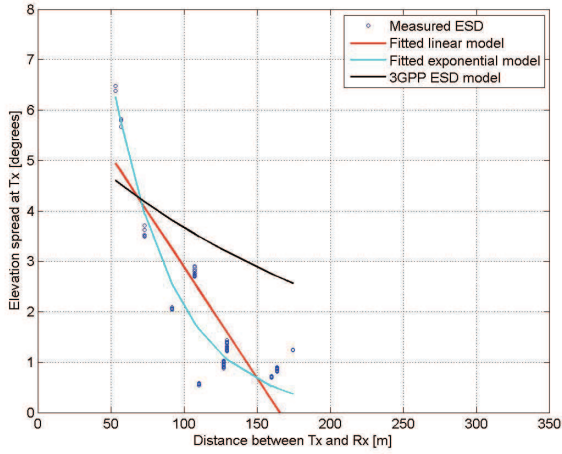


Fig. 5. ESD versus link distance, LOS and Tx height 5 m.

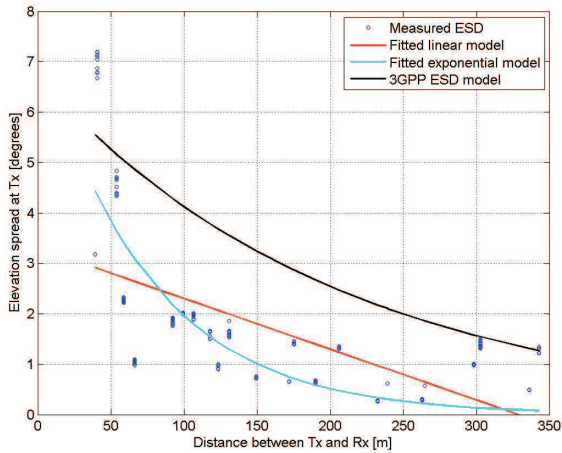


Fig. 6. ESD versus link distance, LOS and Tx height 10 m.

caused by an insufficient number of measurement spots and the lack of dynamic range in the NLOS measurements.

D. Cross-correlation Analysis

The spatial correlations of channel parameters are important in the system level simulations. In order to create correlations between radio links at the system level, the large scale parameters have to be generated with correlation properties [1]. The cross-correlation coefficient is calculated as [1]

$$\rho_{xy} = \frac{C_{xy}}{\sqrt{C_{xx}C_{yy}}}, \quad (6)$$

where C_{xy} is the cross-covariance of parameters x and y and C_{xx} indicates auto-covariance.

The results of cross-correlation coefficients and the statistics of elevation analysis are summarized in Table II, where the mean and the standard deviation of ESD are denoted as μ_{ESD} and σ_{ESD} , respectively. Furthermore, the Table II shows the results for μ_{ESD} and σ_{ESD} reported in [8] and the cross-correlation parameters reported in [12]. According to the

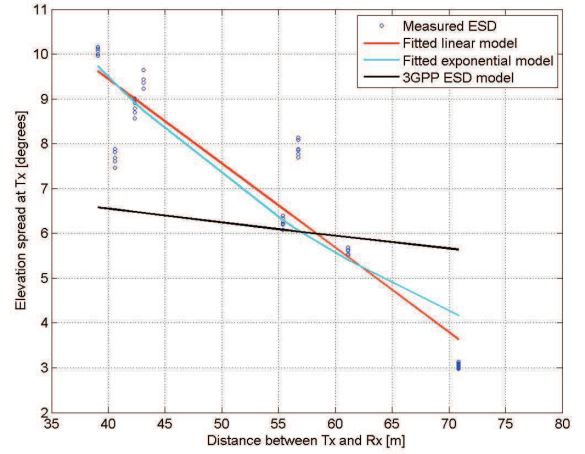


Fig. 7. ESD versus distance, NLOS and Tx height 5 m.

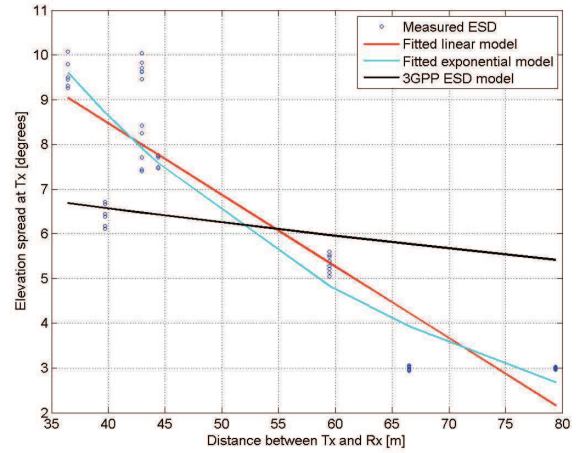


Fig. 8. ESD versus distance, NLOS and Tx height 10 m.

obtained results, the μ_{ESD} decreases, when the Tx antenna height increases.

The σ_{ESD} is higher in the NLOS scenario than in the LOS scenario. This can be also seen from Fig. 3 and Fig. 4. The reason for this is that the contribution of MPCs is weaker in the LOS scenario. Some difference in μ_{ESD} can be noticed between the calculated results and the parameters reported in [8]. In the LOS scenario, the obtained results indicate a smaller μ_{ESD} in comparison to the parameters reported in [8]. On the other hand, the μ_{ESD} obtained for NLOS scenario is larger than in [8]. Furthermore, the observed σ_{ESD} is larger in comparison to the parameters reported in [8]. This is caused by the higher elevation resolution in our measurements.

Some interesting observations concerning cross-correlation coefficients can be noticed from the Table II. The cross-correlation coefficient between the ESD and the azimuth spread of departure (ASD) in the LOS scenario is slightly larger than in [12]. On contrary, the cross-correlation coefficient between the ESD and ASD in the NLOS scenario is smaller in the obtained results than the parameters reported

TABLE II
THE SUMMARY OF MEASUREMENT RESULTS

Parameter	Statistic	LOS		NLOS		Ref. [8], [12]	
		Tx 5 m	Tx 10 m	Tx 5 m	Tx 10 m	LOS	NLOS
ESD \log_{10} (degree)	μ_{ESD}	0.36	0.23	0.86	0.79	0.4	0.6
	σ_{ESD}	0.43	0.28	0.54	0.58	0.2	0.2
EoD distribution		Laplacian		Laplacian			
ESD model	A	21.68	7.52	16.97	14.88		
	B	0.02	0.01	-0.19	-0.16		
	γ (degree)	0.6	0.9	0.9	1.2		
Cross-Correlations	ESD vs ASD	0.6	0.7	0.3	0.1	0.5	0.5
	ESD vs ASA	-0.2	0.1	-0.1	-0.4	0	0
	ESD vs DS	-0.1	0	-0.3	-0.3	0	-0.5

in [12]. The cross-correlation coefficient between the ESD and the azimuth spread of arrival (ASA) is mainly negative. This indicates that as the ESD increases, the ASA decreases. The cross-correlation coefficient between the ESD and delay spread (DS) are almost the same in the obtained results and the parameters reported in [12].

IV. CONCLUSIONS

The radio channel measurements were carried out with 30 x 16 antenna configuration in an urban microcell environment at the center frequency of 2.3 GHz. The Tx antenna heights of 5 m and 10 m were used. An elevation domain analysis was performed for the departure angle estimates. The results showed that the departure angles in the elevation domain can be modelled by the Laplacian distribution. The mean of ESD was decreased as the Tx antenna height was increased. In addition, the difference in ESDs between the LOS and the NLOS propagation environments was significant. The ESD with respect to the distance between the Tx and the Rx was tested against the linear model and the negative exponential model. The distance dependency of ESD was observed to follow negative exponential model and linear model in the LOS and the NLOS case, respectively.

V. ACKNOWLEDGMENT

This research was done under European 7th framework project METIS (Mobile and wireless communications Enablers for the Twenty-twenty Information Society) [13].

REFERENCES

- [1] IST-WINNER, II, "Deliverable 1.1. 2 v. 1.2, WINNER II Channel Models, IST-WINNER2," Tech. Rep., 2008 (<http://projects.celtic-initiative.org/winner+/deliverables.html>), Tech. Rep., 2007.
- [2] ITU-R, "Report ITU-R M.2135 guidelines for evaluation of radio interface technologies for IMT-Advanced," ITU-R, Tech. Rep., 2009.
- [3] Y. Zhang, R. Zhang, S. X. Lu, W. Duan, and L. Cai, "Measurement and modeling of indoor channels in elevation domain for 3D MIMO applications," in *Proc. IEEE Int. Conf. Commun.*, Sydney, Australia, Jun. 10–14 2014, pp. 659–664.
- [4] J. Wang, R. Zhang, W. Duan, S. X. Lu, and L. Cai, "Angular spread measurement and modeling for 3D MIMO in urban macrocellular radio channels," in *Proc. IEEE Int. Conf. Commun.*, Sydney, Australia, Jun. 20–25 2014, pp. 659–664.
- [5] T. A. Thomas, F. W. Vook, E. Visotky, E. Mellios, G. S. Hilton, and A. R. Nix, "3D extension of the 3GPP/ITU channel model," in *Proc. IEEE Vehicular Technology Conf. (VTC)*, Dresden, Germany, pp. 1–5.
- [6] H. M. El-Sallabi and P. Vainikainen, "Impacts of environment and antenna height on angular spread of radiowave propagation in a city street microcell," in *Antennas and Propagation Society International Symposium, IEEE*, vol. 2, Salt Lake City, UT, USA, pp. 1146–1149.
- [7] L. Hentilä, P. Kyösti, and J. Meinilä, "Elevation extension for a geometry-based radio channel model and its influence on MIMO antenna correlation and gain imbalance," in *Proc. Eur. Conf. Ant. Prop.*, Rome, Italy, pp. 2175–2179.
- [8] P. Heino et al., "Deliverable D5.3, WINNER+ Final Channel Models V1.0, CELTIC CP5–026 WINNER+ Project," (http://projects.celtic-initiative.org/WINNER+/deliverables_winnerplus.html), June 2010.
- [9] Elektrobit Ltd, "Tech. rep., propsound - multi-dimensional radio channel sounder.system specifications document," Tech. Rep., 2004.
- [10] A. Stucki and P. Jourdan, "MIMO radio channel parameter estimation using the initialization and search improved SAGE (ISIS) algorithm," in *The 13th Virginia Tech/MPRG Symposium on Wireless Personal Communications*, Blacksburg, Virginia, USA, 4–6 2002.
- [11] 3GPP TR 25.996, "Spatial channel model for multiple input multiple output (MIMO) simulations, v11.0.0," 3GPP, Tech. Rep., 2012.
- [12] 3GPP TSG RAN, "Study on 3D channel model for LTE TR 36.873 (release 12), v2.0.0 (2014-03-09), r1-136084," 3GPP, Tech. Rep.
- [13] METIS, "Mobile and wireless communications enablers for the twenty-twenty information society, EU 7th framework programme, <http://www.metis2020.com>."